



LUND UNIVERSITY  
Faculty of Science

# Shell-model calculations in Ca-region

Weiyi Cui

---

Thesis submitted for the degree of Bachelor of Science  
Project duration: 3 months

Supervised by Gillis Carlsson and Martin Albertsson

Department of Physics  
Division of Mathematical Physics  
June 2018



# Acknowledgements

I would like to thank my supervisor Gillis Carlsson for supporting me with the diploma work. He provided the theme of this thesis to me and helped me throughout the understanding of the basic concepts and writing of the thesis.

I also would like to thank my co-supervisor Martin Albertsson. His patience in trying to solve my confusions is a great encouragement to me.

I also appreciate the supervision from my examiner Claudio Verdozzi. He gave me many suggestions on the specification of the thesis.

# Abstract

In this project, the configuration interaction (CI) method is used to study the nuclear spectra and the interactions between the nucleons in certain nuclei. The NuShellX@MSU code based on the CI method is used to calculate and compare the energy levels of the nuclei  ${}_{20}^{42}\text{Ca}_{22}$ ,  ${}_{22}^{42}\text{Ti}_{20}$ ,  ${}_{21}^{42}\text{Sc}_{21}$ ,  ${}_{24}^{48}\text{Cr}_{24}$  on the basis of the  $J$ -scheme. The calculations test the interactions denoted  $f742pn$  in the  $f7pn$  model space as well as  $fpmcc$ ,  $fpmce$  in the  $fp$  model space. The  $gx1acdpn$  interaction in the  $fppn$  model space is also applied to add Coulomb interactions into the calculations and generate the mirror energy difference (MED). The MEDs are mainly calculated, using the NuShellX@MSU code, between mirror nuclei  ${}_{22}^{42}\text{Ti}_{20}$ - ${}_{20}^{42}\text{Ca}_{22}$  and  ${}_{25}^{48}\text{Mn}_{23}$ - ${}_{23}^{48}\text{V}_{25}$ .

The results of the calculations show that the larger model space that includes more orbits for nucleons gives spectra with more energy states at the price of longer computational time. The different interactions give differences in the nuclear energy levels at a few tens of keV. The rotational behaviour and the backbending phenomenon in the spectra of  ${}_{24}^{48}\text{Cr}_{24}$  are studied. Furthermore, the MEDs' spectra show the breaking of the isospin symmetry between the nucleons. Predictions on the energy levels of  ${}_{26}^{48}\text{Fe}_{22}$  and the MEDs between  ${}_{26}^{48}\text{Fe}_{22}$ - ${}_{22}^{48}\text{Ti}_{26}$  are also made for future experiments by the Lund nuclear structure group.

# List of abbreviations

LDM	Liquid-drop model
SEMF	Semi-empirical mass formula
CI	Configuration interaction
MED	Mirror energy difference

# Contents

<b>I</b>	<b>Introduction</b>	<b>1</b>
<b>1</b>	<b>Nuclear physics</b>	<b>2</b>
1.1	Nuclear composition . . . . .	2
1.2	Nuclear stability and radioactive decay . . . . .	2
1.3	Nuclear Shell Model . . . . .	3
1.4	Mirror energy difference (MED) . . . . .	6
<b>II</b>	<b>Method</b>	<b>8</b>
<b>2</b>	<b>CI method</b>	<b>8</b>
<b>3</b>	<b>NuShellX</b>	<b>9</b>
<b>III</b>	<b>Results</b>	<b>11</b>
<b>4</b>	<b>Example of calculations in Ca-region</b>	<b>11</b>
4.1	Two valence nucleons . . . . .	11
4.2	Eight valence nucleons . . . . .	14
4.2.1	Calculations on ${}^{48}_{24}\text{Cr}_{24}$ . . . . .	14
4.2.2	Predictions on ${}^{48}_{26}\text{Fe}_{22}$ . . . . .	17
4.3	MED calculations . . . . .	20
4.3.1	${}^{42}_{22}\text{Ti}_{20}$ - ${}^{42}_{20}\text{Ca}_{22}$ . . . . .	20
4.3.2	${}^{48}_{25}\text{Mn}_{23}$ - ${}^{48}_{23}\text{V}_{25}$ . . . . .	21
4.3.3	${}^{48}_{26}\text{Fe}_{22}$ - ${}^{48}_{22}\text{Ti}_{26}$ . . . . .	22
<b>IV</b>	<b>Summary and outlook</b>	<b>23</b>

# Chapter I

## Introduction

In nuclear physics, the understanding of the properties of nuclei such as nuclear masses, energy, wave functions and nucleon density distributions is always the key problem. Therefore, many models have been developed to solve these problems and establish the structure of a nucleus.

The liquid-drop model (LDM) suggests an analogy between a nucleus and a liquid droplet. In this model, a nucleus is regarded as collection of neutrons and protons forming a droplet of incompressible fluid. The LDM led to many semiempirical mass formulae, as, e.g. the semi-empirical mass formula (SEMF), which is used to approximate the mass and other properties of a nucleus [1]. A great number of attempts have been made to extend the LDM after that, but it finally comes to a failure with accounting for the “magic numbers” (see the definition in Section 1.4).

The nuclear shell model was proposed and then developed by physicists, including Eugene Paul Wigner, Maria Goeppert Mayer and J. Hans D. Jensen *et al.* in 1949, when the “magic numbers” and other nuclear properties were successfully addressed and explained [2]. After the discovery and development of the shell model, the understanding of the nuclear structure turned into a new, prospective path. The modern nuclear shell model is based on the assumption that the valence protons and neutrons of the nucleus occupy several partially filled quantum states, which is analogous to the atomic shell model [3]. With the emergence of powerful computational facilities, it is possible to understand the complete spectroscopic characterization of nuclear levels. As an example, NuShellX is a set of computer codes for shell-model research, written by Bill Rae [4]. It is used to obtain exact energies, eigenvectors and spectroscopic overlaps for low-lying states in shell-model Hamiltonian matrix calculations, using the method known as configuration interaction (CI). As a set of wrapper codes, NuShellX@MSU is written by Alex Brown, which uses data files for model spaces and Hamiltonians to generate input for NuShellX and convert the NuShellX output into figures and tables for energy levels, gamma decay and beta decay [5].

The main purpose of this project is to gain basic knowledge of the CI method and many-particle theory. The CI method will then be used to study nuclear excitation spectra and calculate the energy levels of many-interacting fermions through the programme NuShellX. The test will mainly focus on the  $^{40}_{20}\text{Ca}$  core (see the reason in Section 1.4) with 2 nucleons added; 8 nucleons added and the CI method will be applied to the calculations of the energy differences between the mirror nuclei (see the definition in Section 2). Comparisons on the calculation results with the experimental results and the results of different numbers of valence nucleons will be analyzed.

Due to limitations of the method and the codes NuShellX@MSU, the calculation time for large number of valence nucleons in relatively large model space can be very long and many Hamiltonians constructed in the codes don't contain complete interactions between nucleons, e.g. Coulomb interaction. Therefore, the interaction types are selected in certain model spaces and the final outputs of the energy levels may have deviations with the experimental results.

# 1 Nuclear physics

## 1.1 Nuclear composition

Between 1908 and 1913, one of the most famous experiments in nuclear physics was pronounced and carried out by Hans Geiger and Ernest Marsden, under the direction of Ernest Rutherford, where alpha particles were fired towards a thin gold foil [6]. The particles scattered in large angles prove that there is an extremely small and dense matter in an atom, which contains most of the mass and heavy positively charged particles. That matter is the nucleus. The nucleus itself contains two types of particles; protons and neutrons. The protons are those heavy positively charged particles as mentioned, which charges are equal to the absolute value of those of the electrons. The symbol of a certain atom is commonly recognized as  ${}^A_ZX$ , where  $Z$  is the atomic number as well as the number of the protons or electrons,  $A$  is the mass number, and the number of the neutrons  $N=A-Z$ .

Protons and neutrons are both fermions, with the half-integer spin. A fermion obeys the Pauli exclusion principle, which states that a given quantum state cannot be occupied by more than one fermion. The properties of the fermion influence the establishment of the nuclear shell model.

## 1.2 Nuclear stability and radioactive decay

Inside a nucleus, there are two forces balancing the nuclear stability; the strong force and the electric force. Only protons will be repelled by the electric force because of the positive charge, and the strong force exists among the interaction of the protons, the interaction of the neutrons and the interaction of the protons-neutrons. Figure 1.1 shows the interactions between the nucleons when there are two neutrons and two protons.

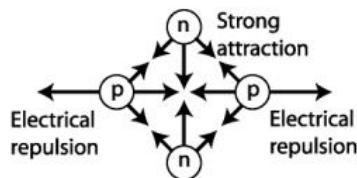


**Figure 1.1** The interactions between the nucleons [7]

The *chart of nuclides* is displayed in Figure 1.2, where every spot in the chart represents a nuclide. The y-axis is labeled neutrons, and the x-axis is labeled protons. The different colors represents different types of nuclei. The black ones represents the stable nuclides, and the other ones are explained in the chart. The solid black line represents the theoretical position of the nuclides that have neutrons and protons with the same number.



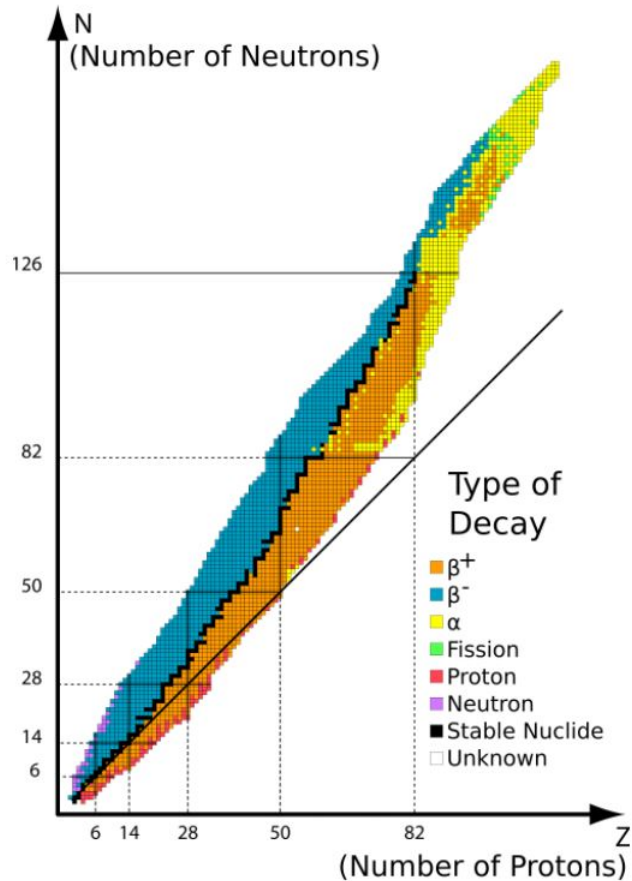


Figure 1.2 Chart of nuclides [8]

The reason for stable nuclei not found beyond  $Z > 82$  is that adding protons in these nuclei will increase the repulsive electric force pushing other protons out of the nucleus without increasing the attractive force.

In Figure 1.2, one can determine where the  $\alpha$  decay,  $\beta$  decay and positron emission or electron capture occurs. These all belong to the radioactivity of the nuclei, as the way the nuclei break up.

$\alpha$  particles are helium nuclei. The  $\alpha$  decay decreases the mass number of the element in order to reach a stable nucleus, so they are found at the top of the nuclear chart.  $\beta$  particles are negatively charged electrons, and the  $\beta$  decay occurs when the nuclei have too many neutrons lie above the belt of stability. Positron  $\beta^+$  emission and electron capture occur below the belt of stability.

### 1.3 Nuclear Shell Model

In the atomic shell model, the electrons are arranged in orbits subject to the laws of quantum mechanics. There are similarities between the atomic structure and the nuclear structure. In 1949, the key role of the spin-orbit coupling in the one-body potential was proposed by Maria Goeppert Mayer [9] and Otto Haxel, J. Hans D. Jensen and Hans Suess [10]. One might think the nucleons would be colliding all the time and fail to maintain a single-particle orbit because of the high density and strong force, but the Pauli exclusion principle states that two or more identical fermions cannot occupy the same quantum state within a quantum system simultaneously, so it supports the shell model picture as strongly bound nucleons becomes confined to their orbits.

There are three potential models which are most commonly used in the study of the nuclear shell model. The first one is the three dimensional harmonic oscillator model. It has the central potential  $V_{HO}$  as

$$V_{HO}(r) = \frac{1}{2}m\omega^2r^2 + const, \quad (1.1)$$

where  $m$  is the nucleon mass and  $\omega$  is the angular frequency of the oscillator.

Figure 1.3 shows the energy levels of the neutrons for a harmonic oscillator potential, where the letters “s, p, d, f, g, h, i...” represent the orbital angular momentum state  $l$  and the numbers before the letters denote the quantum number  $n$ , which refers to the number of times the state  $l$  has appeared. The number on the right of each level is the cumulative number of neutrons that can be put into all the levels up to the indicated level.

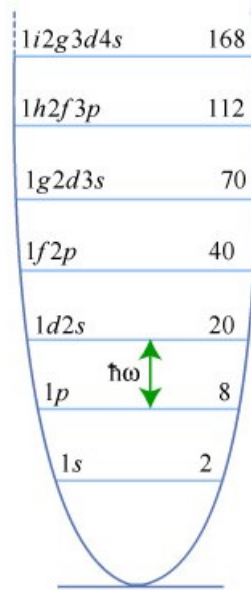


**Figure 1.3** Energy levels of neutrons in a parabolic potential well [11]

The second model is the Woods-Saxon model. The potential is given by the expression:

$$V_{WS}(r) = -\frac{V_0}{1 + \exp[(r - R)/a]} \quad (1.2)$$

where the typical parameter is  $a \approx 0.65$  fm [11].

Figure 1.4 shows the shape of the Woods-Saxon potential and the differences between the proton potential well and neutron potential well. The difference is caused by the Coulomb interaction between the protons.

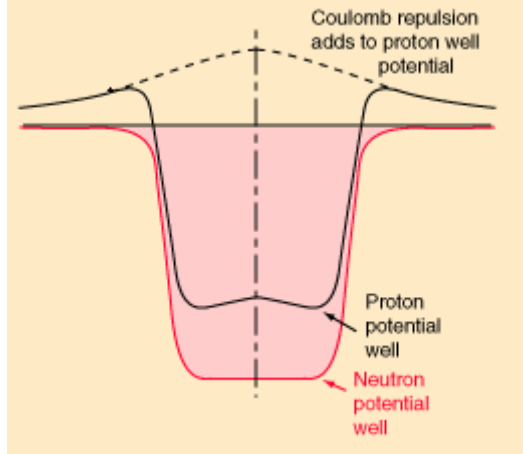


**Figure 1.4** Woods-Saxon potential well for protons and neutrons

The two potential models above contribute to the development of the nuclear shell model, but fail to predict the magic numbers after 20. A nucleus having the magic numbers in either the proton or neutron is particularly stable with the occurrence of strongly bound states. Those most widely recognized magic numbers are 2, 8, 20, 28, 50, 82 and 126 [12]. For example,  $^{40}\text{Ca}$  with 20 neutrons and 20 protons has double magic numbers, which is used as the core in the calculations in Chapter III.

To improve the model, a spin-orbit coupling of the form  $V_{so}(r)\vec{l} \cdot \vec{s}$  is added to the Woods-Saxon potential model:

$$V(r) = -\frac{V_0}{1 + \exp[(r - R)/a]} + V_{so}(r)\vec{l} \cdot \vec{s}. \quad (1.3)$$

It brings the interaction between the orbital angular momentum  $\vec{l}$  and the intrinsic spin angular momentum  $\vec{s}$  of the nucleon. The total angular momentum is defined as  $\vec{j} = \vec{l} + \vec{s}$ . Its quantum number  $j$  has the properties of  $|l - s| \leq j \leq |l + s|$ , and the quantum number  $m_j$  associated with the  $z$  component of  $j$  has the property of  $-j \leq m_j \leq j$ . So each  $j$  has  $2j + 1$   $m_j$  values and each  $j$  orbit can have  $2j + 1$  protons or neutrons. After the introduction of the spin-orbit coupling to the Woods-Saxon potential, the shell model energy levels are shown in Figure 1.5.

The notation on the right side in the Figure 1.5 also has a relationship with the quantum numbers. Taking  $1s_{1/2}$  as an example, “1” represents the quantum number  $n$ , “s” represents  $l = 0$ , which are the same as those mentioned in the harmonic oscillator potential model, and “1/2” represents  $j$ .

The nuclear shell model with spin-orbit coupling makes a successful prediction on the magic numbers and this explains the main gaps between the energy levels. It also indicates the collisions of the fermions in the low-lying nuclear levels are greatly suppressed due to the Pauli principle. The shell model also suggests complex configurations for the nuclei with nucleon numbers between the magic numbers, which require understanding and calculations to learn the nuclear structure better.

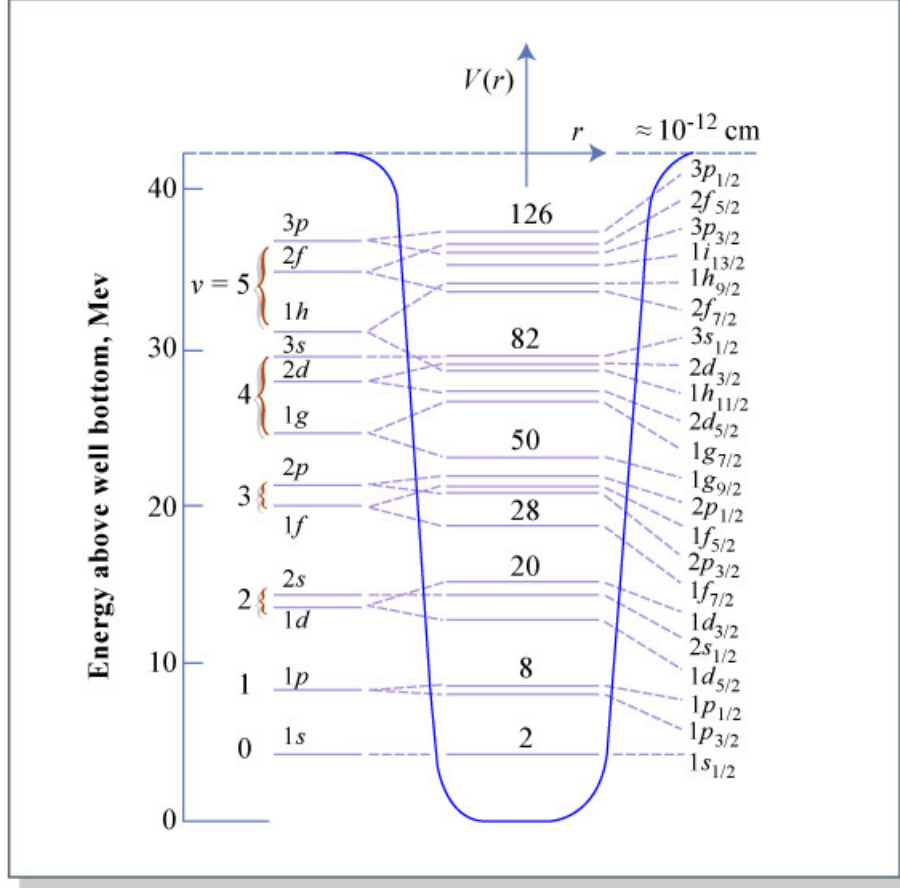


Figure 1.5 Energy levels of nucleons in a potential well with spin-orbit coupling [11]

## 1.4 Mirror energy difference (MED)

In nuclear physics, the isospin symmetry plays an important role because the neutron and the proton have similar mass. In the isospin symmetry,  $t$  is introduced as the isospin quantum number. A nucleon has  $t = 1/2$  and two possible directions in isospin space. The proton has  $t_z = -1/2$  and neutron has  $t_z = +1/2$ . They can be considered different states of the same particle. The states are distinguished by different isospin projections. One assumes that the attractive nuclear force is independent of the charge with the isospin symmetry, so the mirror nuclei, where one's number of protons equals to the other's number of neutrons and one's number of neutrons also equals to the other's number of protons (e.g.  ${}^{42}_{22}\text{Ti}_{20}$  and  ${}^{42}_{20}\text{Ca}_{22}$ ), should have exact symmetry between the analogue states. However, the existence of the electromagnetic effects and small isospin breaking components in the strong force can break this degeneracy, which are proved not only including the Coulomb effects [13]. To study the breaking of the isospin symmetry, one can focus on mirror energy differences (MED), which means the differences between the excitation energy of those analogue states in the pair of mirror nuclide.

With shell-model calculations, the MEDs between the analogue states can be calculated. In this project, the MED of mirror nuclei is defined as

$$MED = E_J(T_z = -T) - E_J(T_z = +T), \quad (1.4)$$

where  $T_z = \sum_{i=1}^A t_z$ . The yrast states (states with a minimum of energy) in  $N \neq Z$  nuclei

and even-even  $N = Z$  nuclei will have total isospin quantum number  $T = |N - Z| / 2$ , so the MED expression defined should be the yrast states of proton-rich nuclei minus neutron-rich nuclei. As the experimental results of some proton-rich nuclei are accessible, one can compare the calculated MEDs to the experimental MEDs to learn about the breaking of the isospin better. The  $f_{7/2}$  shell has been under the focus recently, so in this project, the MEDs between the nuclei  $^{42}\text{Ti}$  &  $^{42}\text{Ca}$ ,  $^{48}\text{Mn}$  &  $^{48}\text{V}$  will be determined with the Coulomb interactions and without the Coulomb interactions using the codes NuShellX, and the prediction on the MEDs between  $^{48}\text{Fe}$  &  $^{48}\text{Ti}$ . The focus will mainly be on the effects of the Coulomb interactions due to the limitations of the codes.

# Chapter II

## Method

The project uses the codes NuShellX to obtain the energy levels and the related spectra of a certain nucleus. The codes written by Bill Rae were developed from old shell model codes OXBASH and NuShell and are based on the method of CI.

### 2 CI method

The method of CI is more commonly found in quantum chemistry to calculate the properties of many-electron system. It is basically a way to find solutions of the Schrödinger equation for a many-interacting-particle system [14].

In this work, we calculate the energy levels of the nuclei with few more nucleons in the low-lying nuclear levels outside the core of a magic nucleus. These low-lying nuclear levels outside the core are in shells called valence shells, and the valence nucleons can thus appear and interact in the different states causing different “configurations”. In other words, the wavefunction of the nucleus is expanded as a linear combination of several many-particle basis states, which represent the configurations, and the states can mix with each other to minimize the energy, which involves the interaction.

To obtain the energy levels of a certain nucleus, one should solve the many-body Schrödinger equation and find the eigenvalues of the Hamiltonian describing the related many-interacting-particle system.

The Schrödinger equation is defined as

$$\hat{H}\Psi(1, 2, \dots, N) = E\Psi(1, 2, \dots, N). \quad (2.1)$$

The Hamiltonian in the shell model can be denoted as

$$\hat{H} = \hat{H}_1 + \hat{H}_2 = \sum_{i=1}^N \left[ -\frac{\hbar^2}{2m} \nabla_i^2 + V(r) \right] + \frac{1}{2} \sum_{j \neq i}^N V(\mathbf{r}_i, \mathbf{r}_j), \quad (2.2)$$

where  $\hat{H}_1$  is a one-particle operator composed of the kinetic energy and the mean field potential, and  $\hat{H}_2$  is a two-particle operator with the residual interaction between the nucleons.

When one neglects the interaction part, the equation will only have a single-particle Hamiltonian, which is much simpler, and the eigenfunction will be a single Slater determinant, which represents the wavefunction. However, one should include the interaction between the nucleons in the calculation in this project, and the Hamiltonian should be diagonalized in a finite subspace. The diagonalization method often used is called Lanczos procedure, where the matrix is diagonalized more efficiently than with traditional methods.

One expands  $\Psi$  on a set of basis states as

$$\Psi = \sum_i \varphi_i \cdot c_i. \quad (2.3)$$

The final step is to solve the eigenvalue problem of the matrix as

$$\bar{H} = \begin{bmatrix} \langle \varphi_1 | \hat{H} | \varphi_1 \rangle & \dots & \langle \varphi_1 | \hat{H} | \varphi_N \rangle \\ \vdots & \ddots & \vdots \\ \langle \varphi_N | \hat{H} | \varphi_1 \rangle & \dots & \langle \varphi_N | \hat{H} | \varphi_N \rangle \end{bmatrix}. \quad (2.4)$$

### 3 NuShellX

To calculate the energy levels of certain nuclei using the CI method, the NuShellX codes are used. The codes use a  $J$ -coupled proton-neutron basis, and the matrix is based on  $J$ -scheme allowing the dimensions of up to the order of 100 million [5]. The total angular momentum  $J$  is coupled by the spin of the neutrons,  $j_n$  with the spin of the protons,  $j_p$ , and obeys the general rule

$$|j_p - j_n| \leq J \leq |j_p + j_n|. \quad (3.1)$$

In this project, NuShellX@MSU is used. It is a set of wrapper codes with the user-friendly interface shown in Figure 4.1 and provides outputs with figures and tables for the calculated energy levels.

In the program, one should choose the related model space and interaction type for the nucleus to be calculated. The model spaces and interaction types are provided in the origin folder of the program. Different model spaces include different orbits, and one model space can also have model space interactions that are different from each other. The model space interactions are constructed using advanced methods to reduce the valence space. Some of the interactions have also been empirically adjusted further to reproduce data. In the following we will not distinguish the two types but rather apply them to describe spectra in order to get an idea of the usefulness of CI calculations for the Ca-region.

```

weiyicui@e123:~/Documents/test$ shell

using label.dat      from area /nfs/users2/weiyicui/Documents/aaa/nushellx/sps/

name for batch file (h=help) :Ca42

option (lpe, den, help or st) :lpe
model space (*.sp) name: f7pn
any restrictions (y/n) :
interaction (*.int) name : f748pn
number of protons : 20

        number of valence protons =    0
number of nucleons : 42
        number of valence nucleons =    2
min J, max J, del J :0.,6.
parity (0 for +) (1 for -) (2 for both) :0
number of proton partitions =          1
number of neutron partitions =         1

approximate time to converge 10 states with 4-core (2.6 GHz)

```

Figure 4.1 Typical interface of NuShellX@MSU

The focus on this project will be mainly on the calculations of  $^{42}\text{Ca}$ ,  $^{42}\text{Ti}$ ,  $^{42}\text{Sc}$ ,  $^{48}\text{Cr}$ , and  $^{48}\text{V}$  in the model space denoted  $f7pn, fp$  and  $fppn$ , which are only symbols used to distinguish the model spaces. The  $f7pn$  model space includes  $1f_{7/2}$  orbits, the  $fp$  model space includes  $1f_{7/2}$ ,  $2p_{3/2}$ ,  $1f_{5/2}$ ,  $2p_{1/2}$  orbits, and the  $fppn$  will be taken into consideration during the calculation of the MEDs, which includes  $p1f_{7/2}$ ,  $2p_{3/2}$ ,  $1f_{5/2}$ ,  $2p_{1/2}$  orbits and  $n1f_{7/2}$ ,  $2p_{3/2}$ ,  $1f_{5/2}$ ,  $2p_{1/2}$  orbits. As the Coulomb interactions are introduced in the  $fppn$  model space, the notations “ $p$ ” and “ $n$ ” are added before the orbits to show the differences between the calculation of protons and neutrons. The prediction of the energy levels of  $^{48}\text{Fe}$  can also finally be obtained using the program.

When calculating the nucleus with 8 valence nucleons in a larger model space, such as  $fp$  and  $fppn$ , the configurations can be very complicated and the matrix of the Hamiltonian can be extremely large. For example, consider four valence protons in the  $fp$  model space, the number of configurations can reach 4845, and if another four valence neutrons are taken into consideration, the total number of configurations can be  $4845^2 = 2.347 \times 10^7$ , so the dimension of the matrix can reach 20 million. The program uses states with good angular momentum as basis states (j-scheme). This allows treating each value of  $J$  separately, which greatly reduces the size of the matrices to be considered. The largest calculations performed in this project usually took one night on a standard desktop computer.



# Chapter III

## Results

### 4 Example of calculations in Ca-region

#### 4.1 Two valence nucleons

First, the nuclei with two valence nucleons outside the  $^{40}\text{Ca}$  core are considered.

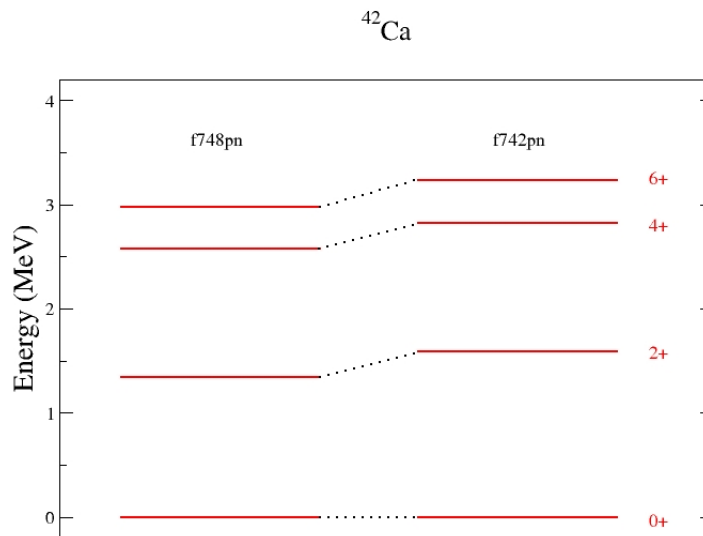


**Figure 5.1** Energy levels of  $^{42}\text{Ca}$  with interaction type  $f748pn$  and  $f742pn$  in the model space  $f7pn$

Figure 5.1 shows the energy levels of  $^{42}\text{Ca}$ , which has two valence neutrons. The calculations were carried out in the  $f7pn$  model space with the  $f742pn$  and  $f748pn$  interactions. The notations on the right side of the spectra represent the  $J$  and the parity. As  $^{42}\text{Ca}$  has 2 valence neutrons and the model space is in  $1f_{7/2}$  orbit, the maximum of  $J$  should equal to  $7/2 + 5/2 = 6$  according to the Pauli principle. The Pauli principle is also the reason why only even  $J$  is observed in the spectra, but it is complicated and beyond the discussion in this thesis. For all the orbits considered in this project, the quantum number  $l$  is odd, and since the number of valence nucleons calculated is even, the parity  $\pi = (-1)^{l_1} \dots (-1)^{l_n}$  will only be positive. It can be seen that in one certain model space, different interaction types can lead to different calculated results of the energy levels, so it is essential to find an interaction type with the closest results to the experimentally obtained levels.

Figure 5.2 shows a comparison of calculated results of  $^{42}\text{Ca}$  between the model space  $f7pn$  and  $fp$ . The figures are the direct outputs of the program with the experimental results shown in the left panel. The reason why there are more energy levels in the  $fp$  model space is that more orbits are included which provide more configurations for one certain  $J$ . Thus, one can find some levels with the same length of line in the output (the length of the lines are proportional to  $J$ ). The blue lines in the experimental spectra

represent the levels of negative parities, which cannot be found in the calculations in this project because we use the  $^{40}\text{Ca}$  as the core. The blue lines and extra red lines come from the excitation of the nucleons from the orbits inside the  $^{40}\text{Ca}$  core, but only orbits outside the core are considered in this project. The black dots in the experimental spectra may be levels where  $J$  is unknown.

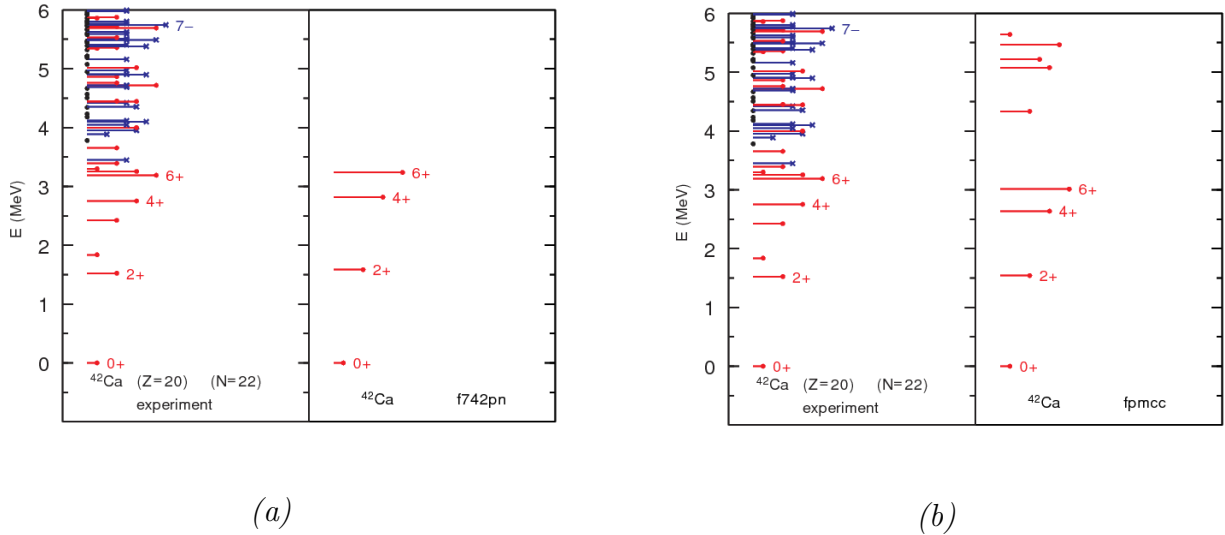


**Figure 5.2** Calculated energy levels of  $^{42}\text{Ca}$  with interaction type (a)  $f742pn$  in the model space  $f7pn$ ; (b)  $fpmcc$  in the model space  $fp$

After the comparison among all the interaction types in the the model space  $f7pn$  and  $fp$ , the interaction type  $f742pn$  in the model space  $f7pn$  and  $fpmcc$  in the model space  $fp$  are considered to fit the experimental results best, illustrated in Figure 5.3, where only the lowest energy levels for each  $J$  are taken into the comparison. The data are shown in Table 5.1.

**Table 5.1** Data of experimental energy levels of  $^{42}\text{Ca}$  [15] and calculated levels in  $f742pn$  and in  $fpmcc$

$^{42}\text{Ca}$	$J$			
	0+	2+	4+	6+
$E_{exp}(\text{MeV})$	0.0	1.52471	2.75240	3.18926
$E_{f742pn}(\text{MeV})$	0.0	1.586	2.817	3.237
$E_{fpmcc}(\text{MeV})$	0.0	1.542	2.636	3.012

The 2+ levels of  $^{42}\text{Ca}$  in  $f742pn$  and  $fpmcc$  are both higher than the experimental results. For the interaction  $f742pn$ , the values of 4+ and 6+ levels are larger than the experimental results, and for  $fpmcc$ , the values of 4+ and 6+ levels are smaller than the experimental results. The relationships can be compared to the following calculations in the nuclei with more valence nucleons.

The mirror nucleus of  $^{42}\text{Ca}$  is  $^{42}\text{Ti}$ , with two valence protons. The calculation results of  $^{42}\text{Ti}$ 's energy levels turn out to be exactly the same as the energy levels of  $^{42}\text{Ca}$  in the two model spaces  $f7pn$  and  $fp$  using the NuShellX codes, which means no Coulomb interaction is included in all of the interaction types in these two model spaces. This can be seen using the  $f742pn$  as an example in Figure 5.4.

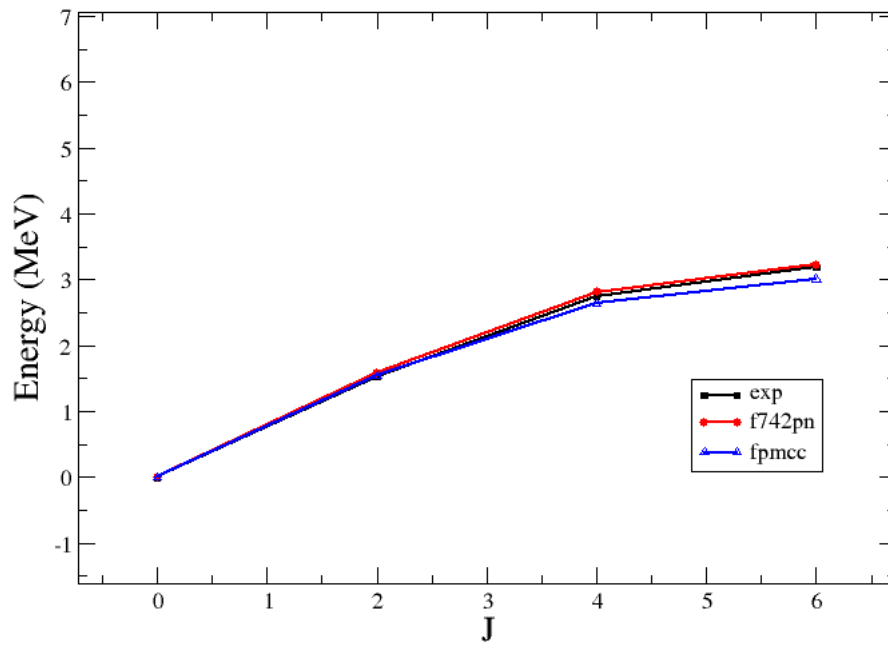


**Figure 5.3** Experimental energy levels of  $^{42}\text{Ca}$  and calculated levels in  $f742pn$  and in  $fpmcc$

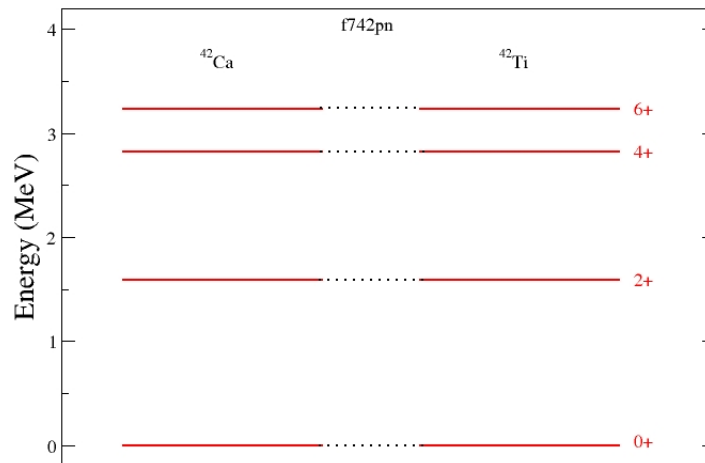


**Figure 5.4** Calculated energy levels of  $^{42}\text{Ca}$  and  $^{42}\text{Ti}$  using  $f742pn$

The energy levels of  $^{42}\text{Sc}$  are also calculated in the two model spaces  $f7pn$  and  $fp$ . The values of the same  $J$  levels are the same with  $^{42}\text{Ca}$  and  $^{42}\text{Ti}$  using the same interaction type in these two model spaces, but Figure 5.5 shows that there are more  $J$  values in  $^{42}\text{Sc}$  compared to Figure 5.2 (b). We choose the  $fpmcd$  interaction type in the  $fp$  model space here as it shows the clearest output spectra. In the nucleus of  $^{42}\text{Sc}$ , the two valence fermions are one proton and one neutron, therefore, the Pauli principle imposes no limitations on the spins of the fermions. Therefore, the maximum of the total angular momentum  $J = j_p + j_n = 7/2 + 7/2 = 7$ .

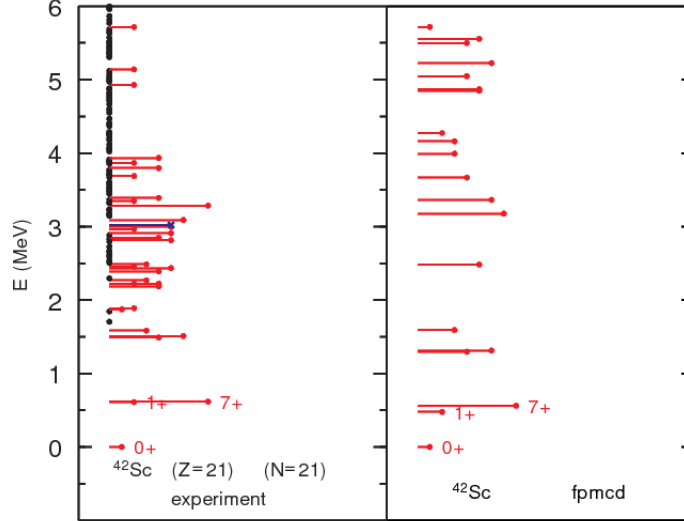


**Figure 5.5** Calculated energy levels of  $^{42}\text{Sc}$  using  $fpmcd$  in  $fp$  model space

## 4.2 Eight valence nucleons

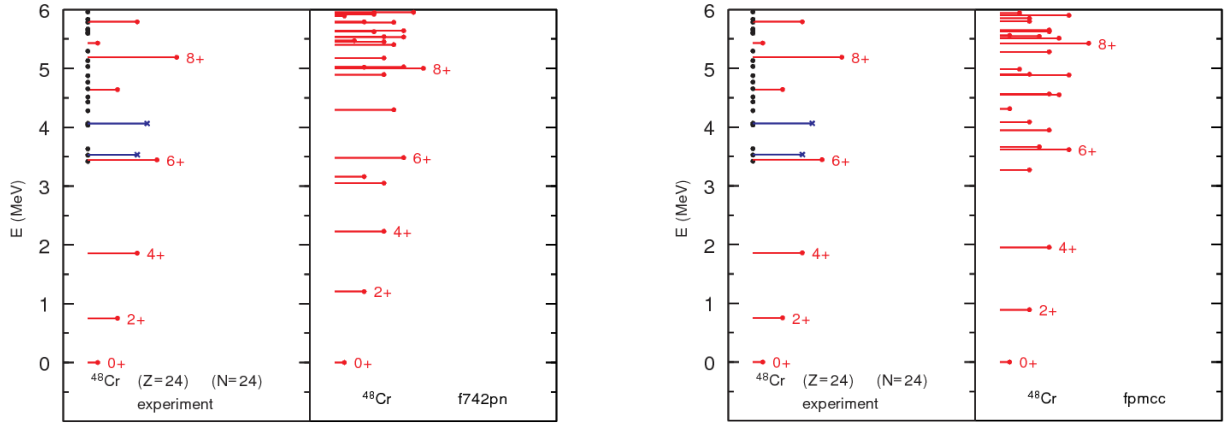
### 4.2.1 Calculations on $^{48}_{24}\text{Cr}_{24}$

As the programme has a good performance in the calculation of energy levels of the two-valence-nucleon nuclei with the errors of tens of keV compared to the experimental results, we will test the calculations on eight-valence-nucleon nuclei.  $^{48}\text{Cr}$  has eight valence nucleons—four neutrons and four protons—outside the  $^{40}\text{Ca}$  core. Due to the limitations of the long calculation time with the program on nuclei with more nucleons, the  $f742pn$  Hamiltonian in model space  $f7pn$  and  $fpmcc$  Hamiltonian in model space  $fp$  are applied to calculate the energy levels of  $^{48}\text{Cr}$  as they are used in the calculations of  $^{42}\text{Ca}$  and  $^{42}\text{Ti}$ . As four neutrons and four protons are included, the total angular momentum is in the scale of  $0 \leq J \leq |j_p + j_n| = (7/2 + 5/2 + 3/2 + 1/2) + (7/2 + 5/2 + 3/2 + 1/2) = 16$ . The outputs of the calculations are shown in the Figure 5.6.

**Table 5.2** Data of experimental energy levels of  $^{48}\text{Cr}$  [16] and calculated levels in  $f742pn$  and in  $fpmcc$

$^{48}\text{Cr}$					
$J$	0+	2+	4+	6+	8+
$E_{exp}$ (MeV)	0.0	0.75219	1.85847	3.4449	5.1883
$E_{f742pn}$ (MeV)	0.0	1.207	2.230	3.483	5.002
$E_{fpmcc}$ (MeV)	0.0	0.889	1.953	3.615	5.4267
$J$	10+	12+	14+	16+	
$E_{exp}$ (MeV)	7.0638	8.4108	10.2797	13.3088	
$E_{f742pn}$ (MeV)	6.442	7.874	10.238	13.551	
$E_{fpmcc}$ (MeV)	7.432	9.051	11.207	14.807	

The program itself only collects experimental levels of the nuclei under 6 MeV, so the output figures will only show those under-6-MeV calculated levels. The details of the calculated energy levels is displayed in Table 5.2.



(a)

(b)

**Figure 5.6** Calculated energy levels of  $^{48}\text{Cr}$  with interaction type (a)  $f742pn$  in the model space  $f7pn$ ; (b)  $fpmcc$  in the model space  $fp$

To display the difference between the experimental results and the calculated results more directly, the plots of data are illustrated in Figure 5.7.

It can be seen from Figure 5.7 that for the lowest energy levels for each  $J$ , the results from  $fpmcc$  fit the experimental results better in low  $J$ 's while results from  $f742pn$  are larger, and when  $J$  increases, the results from  $fpmcc$  go larger than the experimental results while results from  $f742pn$  tend to fit the experimental results better. Compared with the results from Figure 5.3, the performance of one certain interaction type for different nuclei can be different, and since the calculations of  $^{48}\text{Cr}$  involve more nucleons, the differences between different interaction types can be more obvious. The  $fpmcc$  Hamiltonian includes more orbits, so there will be more configurations calculated using  $fpmcc$  than using  $f742pn$ , which is displayed in Figure 5.7.

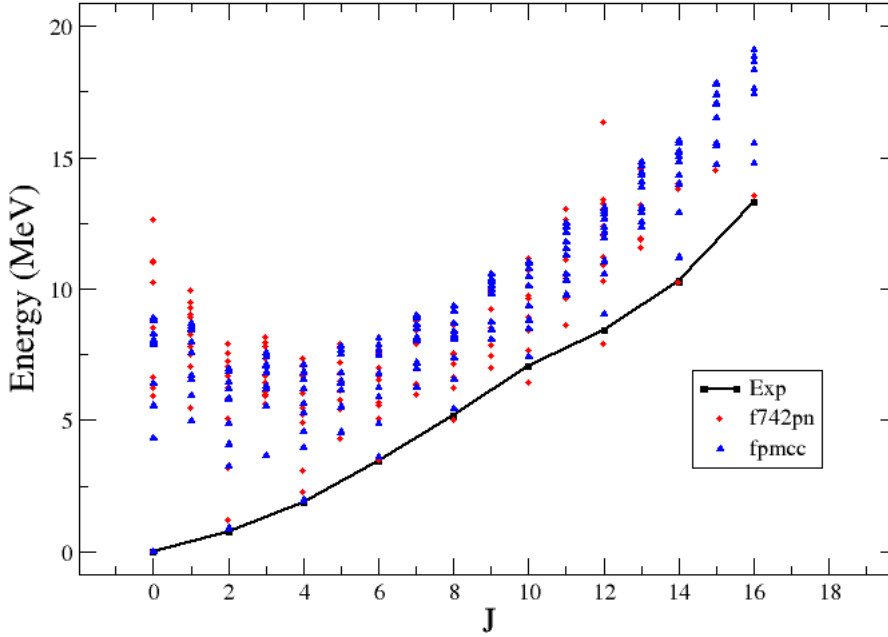


**Figure 5.7** Experimental energy levels of  $^{48}\text{Cr}$  and calculated levels in  $f742pn$  and in  $fpmcc$

Another charming characteristic in Figure 5.7 is that the rotational behavior and backbending displayed in the  $T = 0$  yrast band. The rotational behavior can be obtained by analyzing the ratio  $\left| \frac{Q_0(S)}{Q_0(B)} \right|$  and  $\frac{E(4^+)}{E(2^+)}$  [17], where

$$\frac{Q_0(S)}{Q_0(B)} = -\frac{7}{2} \sqrt{\frac{5}{16\pi}} \frac{Q(2^+)}{\sqrt{B(E2)}}. \quad (4.1)$$

$Q_0$  is the intrinsic quadrupole moment.  $Q_0(S)$  represents the static  $Q_0$ , and  $Q_0(B)$  represents the  $Q_0$  related to the  $E2$  transition strength  $B(E2)$ . In simple rotational models,  $\left| \frac{Q_0(S)}{Q_0(B)} \right|$  should equal to unity. The  $\frac{E(4^+)}{E(2^+)}$  is used to measure how close the nucleus is to the vibrational limit of 2/1, or the rotational limit of 10/3.

As this part is far beyond my knowledge in nuclear physics, the ratio and parameters will only be used to prove the rotational behavior of  $^{48}\text{Cr}$ . For  $^{48}\text{Cr}$ , the experimental data of  $Q(2^+) = -33.271 \text{ e fm}^2$ , and  $B(E2) = 1378.4 \text{ e fm}^2$  [18]. Thus,  $\frac{Q_0(S)}{Q_0(B)} = 0.98923$  for  $^{48}\text{Cr}$  experimentally, which is close to 1, indicating the rotational behavior of  $^{48}\text{Cr}$ .  $\frac{E(4^+)}{E(2^+)} = 2.4707$ , which is between vibrational and rotational.

At  $J = 10$ , the phenomenon backbending appears, which is an irregularity in the spectra. In heavier nuclei, the backbending is caused by e.g. a band crossing, but the reason for this backbending in  $^{48}\text{Cr}$  still needs further research [19].

To present a better fit to the experimental results, the  $fpmce$  Hamiltonian in the model space  $fp$  is used, which is a modification to the  $fpmcc$  Hamiltonian [20]. The comparison of the calculated energy levels is displayed in Figure 5.8. It shows that the results of  $fpmce$  fit the experimental results better than  $fpmcc$ , which can be also reflected in Table 5.3.

**Table 5.3** Differences between experimental energy levels of  $^{48}\text{Cr}$  and calculated levels in *fpmce* and *fpmcc*

$^{48}\text{Cr}$					
$J$	0+	2+	4+	6+	8+
$\Delta E_{fpmce}(\text{MeV})$	0.0	-0.0648	0.04347	0.07890	0.1113
$\Delta E_{fpmcc}(\text{MeV})$	0.0	-0.137	-0.09453	-0.1701	-0.2384
$J$	10+	12+	14+	16+	
$\Delta E_{fpmce}(\text{MeV})$	0.1138	0.0128	-0.2413	-0.4972	
$\Delta E_{fpmcc}(\text{MeV})$	-0.3682	-0.6402	-0.9273	-1.4982	

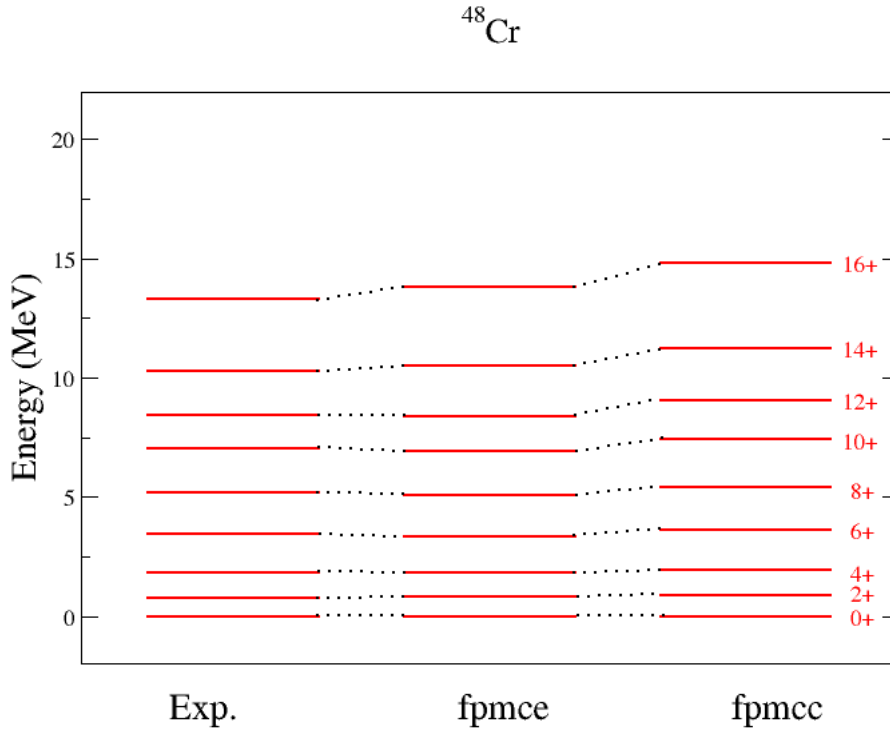


**Figure 5.8** Calculated energy levels of  $^{48}\text{Cr}$  using *fpmce* and *fpmcc*

#### 4.2.2 Predictions on $^{48}_{26}\text{Fe}_{22}$

In the chart of nuclides on National Nuclear Data Center online [21], the energy levels of many proton-rich nuclides have not been reached through experimental methods yet, including  $^{48}\text{Fe}$  with the same mass number as  $^{48}\text{Cr}$  which has been calculated in Section 5.2.1. However, with the approach through NuShellX codes, some predictions of the energy levels of the nuclide  $^{48}\text{Fe}$  can be proposed.

The Figure 5.9 shows the calculated energy levels of  $^{48}\text{Fe}$  using the *fpmce* Hamiltonian in the *fp* model space, which has been proved to have a good fit to the experimental results for  $^{48}\text{Cr}$  in Section 5.2.1.

The lowest energy levels of each  $J$  for  $^{48}\text{Fe}$  calculated by the *fpmce* interaction are listed in Table 5.4.

**Table 5.4** Calculated energy levels of  $^{48}\text{Fe}$  using *fpmce* in *fp* model space

$^{48}\text{Fe}$							
$J$	0+	1+	2+	3+	4+	5+	6+
$E_{fpmce}$ (MeV)	0.0	3.798	1.117	3.172	2.446	4.507	3.340
$J$	7+	8+	9+	10+	11+	12+	
$E_{fpmce}$ (MeV)	5.357	4.722	6.375	6.436	7.655	8.410	

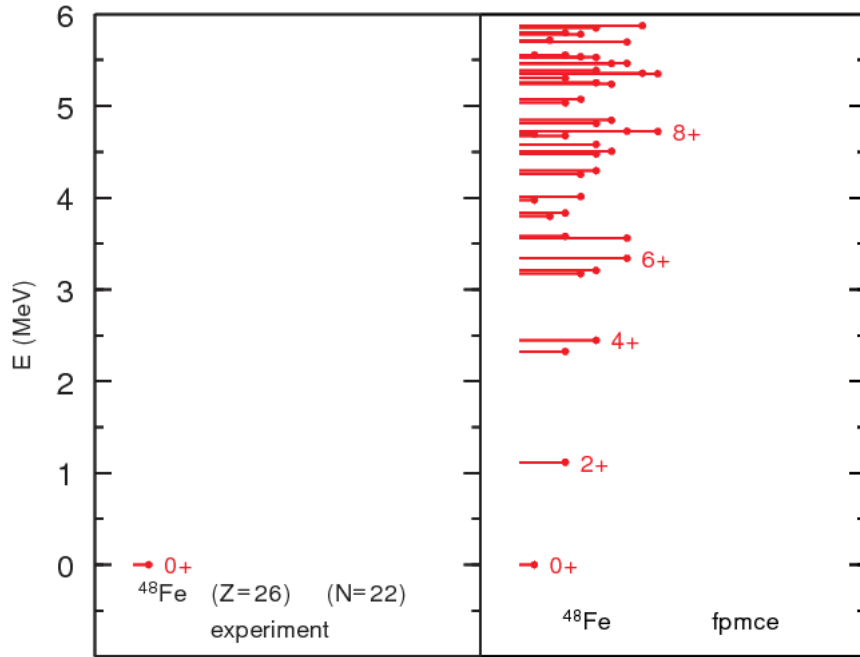


**Figure 5.9** Calculated energy levels of  $^{48}\text{Fe}$  using *fpmce* in *fp* model space

However, in Section 5.1, the interaction types included in the *f7pn* and *fp* model space have been proved to neglect the Coulomb interaction in the nucleons. Therefore, another interaction type in other model spaces should be introduced to calculate the energy levels of  $^{48}\text{Fe}$  taking the Coulomb effects into consideration. The *gx1acdpn* interaction in the *fppn* model space contains Coulomb interaction added based on the *gxpfla* interaction [22]. The *gx1acdpn* interaction is first applied to the calculations on  $^{48}\text{Cr}$ , the result is shown in Figure 5.10.



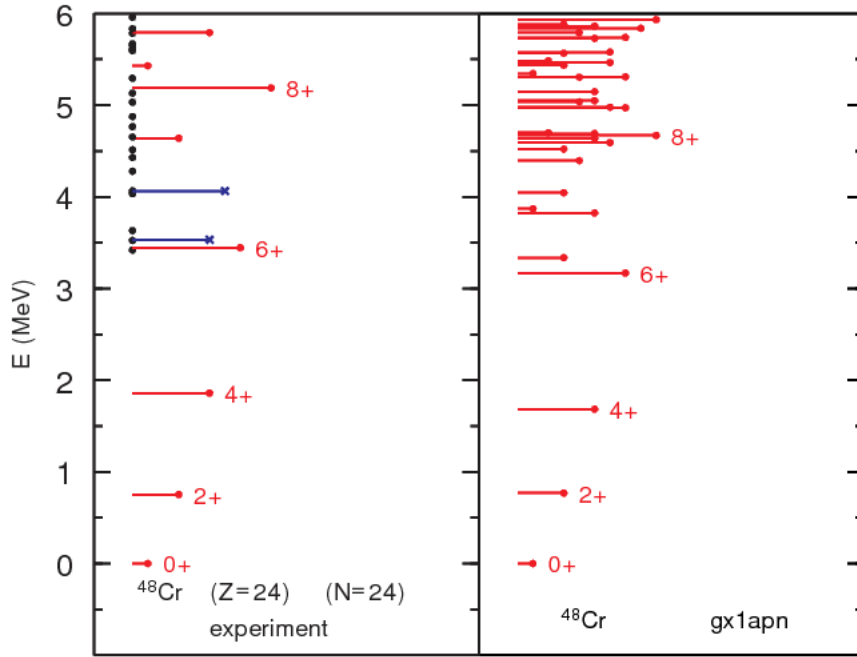


**Figure 5.10** Calculated energy levels of  $^{48}\text{Cr}$  using  $gx1acdpn$  in  $fppn$  model space

One should note that the interaction name is displayed wrongly as  $gx1apn$  in the output spectra using  $gx1acdpn$  interaction due to the program's own error. The energy levels are lower than the experimental results on  $^{48}\text{Cr}$  when  $J = 4, 6, 8$ , which can be observed from the spectra directly.

The  $gx1acdpn$  interaction applied to  $^{48}\text{Fe}$  has the output spectra in Figure 5.11.

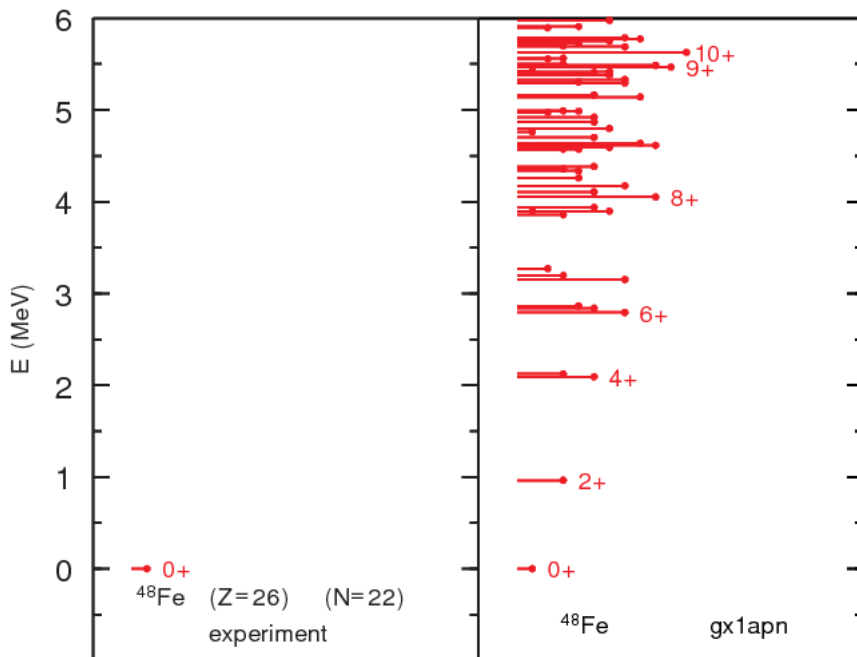


**Figure 5.11** Calculated energy levels of  $^{48}\text{Fe}$  using  $gx1acdpn$  in  $fppn$  model space

The lowest energy levels of each  $J$  for  $^{48}\text{Fe}$  calculated by  $gx1acdpn$  interaction are

listed in Table 5.5.

**Table 5.5** Calculated energy levels of  $^{48}\text{Fe}$  using  $gx1acdpn$  in  $fppn$  model space

$^{48}\text{Fe}$							
$J$	0+	1+	2+	3+	4+	5+	6+
$E_{gx1acdpn}$ (MeV)	0.0	3.272	0.964	2.863	2.092	3.898	2.793
$J$	7+	8+	9+	10+	11+	12+	
$E_{gx1acdpn}$ (MeV)	4.638	4.051	5.468	5.628	6.772	7.675	

It can be seen from the calculation results directly through Table 5.4 and Table 5.5 that with Coulomb interactions added, the energy levels become lower, which can be understood as a result of the repulsive Coulomb effects between the protons. The calculated energy levels of  $^{48}\text{Fe}$  with and without the Coulomb interaction using the code NuShellX@MSU can be used as a reference for the experiments on the measurement of the energy levels of  $^{48}\text{Fe}$  in the future.

### 4.3 MED calculations

#### 4.3.1 $^{42}\text{Ti}_{20}$ - $^{42}\text{Ca}_{22}$

As no Coulomb interactions are involved in the interaction types in  $f7pn$  and  $fp$  model space, according to the isospin symmetry, the energy levels of the mirror nuclei should be exactly the same as we have shown in Section 5.1. To find out the breaking of the isospin symmetry, interaction types including the Coulomb interactions should be introduced to calculate the energy levels of the mirror nuclei, which is the  $gx1acdpn$  interaction in the  $fppn$  model space used in Section 5.2.2. The focus of the MED will be on the nuclei  $^{42}\text{Ti}$  and  $^{42}\text{Ca}$  first.

Figure 5.12 shows the experimental and calculated MEDs of  $^{42}\text{Ti}$  and  $^{42}\text{Ca}$ .

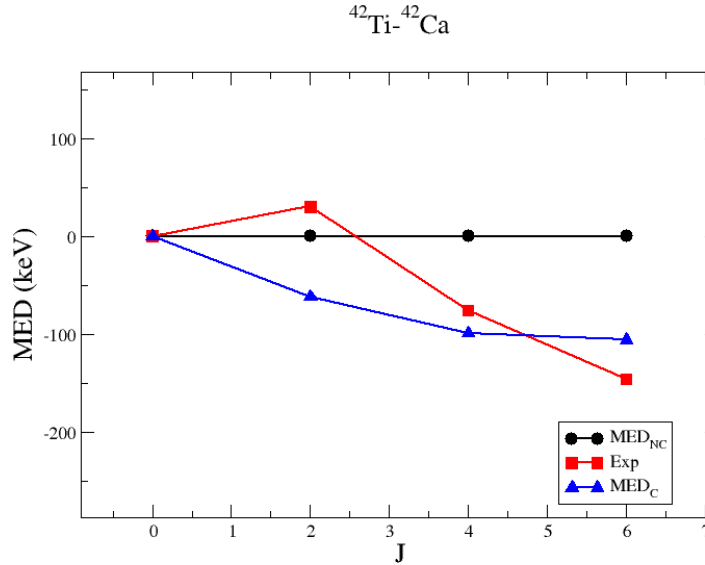


**Figure 5.12** Experimental and calculated MEDs of  $^{42}\text{Ti}$  and  $^{42}\text{Ca}$ . MED<sub>NC</sub> represents the calculated MED with no Coulomb interactions; MED<sub>C</sub> represents the calculated MED with Coulomb interactions

From Figure 5.12, one can see with the Coulomb interactions involved, the MED of  $^{42}\text{Ti}$  and  $^{42}\text{Ca}$  remains negative and has a decreasing tendency. Comparing with the MED with no Coulomb interactions remaining 0, the  $\text{MED}_C$  indicates there should be the breaking of the isospin symmetry in mirror nuclei. However, as Figure 5.12 shows the calculated MED with Coulomb interactions still have large differences with the experimental MED, one can conclude that the Coulomb interactions may only be part of the cause of isospin symmetry breaking, where the strong nuclear force can also be considered as the component of the breaking, or the interaction types used does not take all the possible effects into consideration. The MED can be composed of a monopole Coulomb component, a multipole Coulomb component, and an isospin breaking nuclear interaction component [23], any of which can be the missing part in the interaction type used in this project.

For  $^{42}\text{Ti}$ , the breaking and alignment of the  $1f_{7/2}$  proton pair form the excited states, where the average distance of the protons increases. This leads to the Coulomb energy decrease when the spin increases for the two protons, and  $^{42}\text{Ca}$  does not have this effect. One can express the MED between  $^{42}\text{Ti}$  and  $^{42}\text{Ca}$  in the following form

$$\text{MED} = E^{2p}(J) - E^{2n}(J). \quad (4.2)$$

So with the decrease of  $E^{2p}$  when the spin increases, the MED should decrease as well. This conclusion fits the calculated results well, but for the experimental results, there comes the  $J = 2$  anomaly. According to the Ref. [24], the  $J = 2$  anomaly is present throughout the  $1f_{7/2}$  shell, not only for the  $^{42}\text{Ti}$  and  $^{42}\text{Ca}$  pair. The monopole Coulomb contributions can be the reason, but it has not been proved in the  $A=42$  mirror nuclei.

#### 4.3.2 $^{48}_{25}\text{Mn}_{23}$ - $^{48}_{23}\text{V}_{25}$

Figure 5.13 shows the experimental and calculated MEDs of  $^{48}\text{Mn}$  and  $^{48}\text{V}$ .

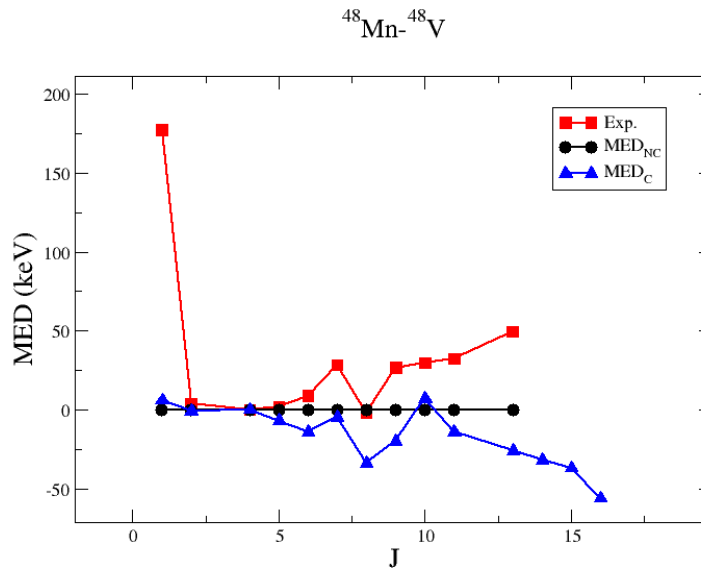


**Figure 5.13** Experimental and calculated MEDs of  $^{48}\text{Mn}$  and  $^{48}\text{V}$ .  $\text{MED}_{\text{NC}}$  represents the calculated MED with no Coulomb interactions;  $\text{MED}_C$  represents the calculated MED with Coulomb interactions

The breaking of the isospin symmetry brought by the Coulomb interactions and the limitations of the interaction type are also seen in Figure 5.13. Among the experimental results, the deviation of the MED between  $^{48}\text{Mn}$  and  $^{48}\text{V}$  on  $J = 2$  is very pronounced. However, this large MED may come from the original data from the National Nuclear Data Center [25], where the measurement of the energy levels of  $^{48}\text{Mn}$  are uncertain experimentally. So the MED on  $J = 2$  given by the calculation can be a prediction to some extents. Possibilities that the deviation on  $J = 2$  is well described by the experimental results still exists.

Since the MEDs are very complicated with the mirror nuclei  $^{48}\text{Mn}$  and  $^{48}\text{V}$ , it is difficult to figure out how the components contribute on the changes of the MED. But one can find the similar tendency between the experimental MEDs and the calculated MEDs with Coulomb interactions, with the calculated results adding some positive effects which may be caused by the nuclear force components. With the experimental data of  $^{48}\text{Mn}$  only available under  $J = 13+$ , the MEDs above  $J = 13+$  spin can be estimated from Figure 5.13 and show a continuous decrease.

### 4.3.3 $^{48}_{26}\text{Fe}_{22}$ - $^{48}_{22}\text{Ti}_{26}$

Figure 5.14 shows the calculated MEDs of  $^{48}\text{Fe}$  and  $^{48}\text{Ti}$ .

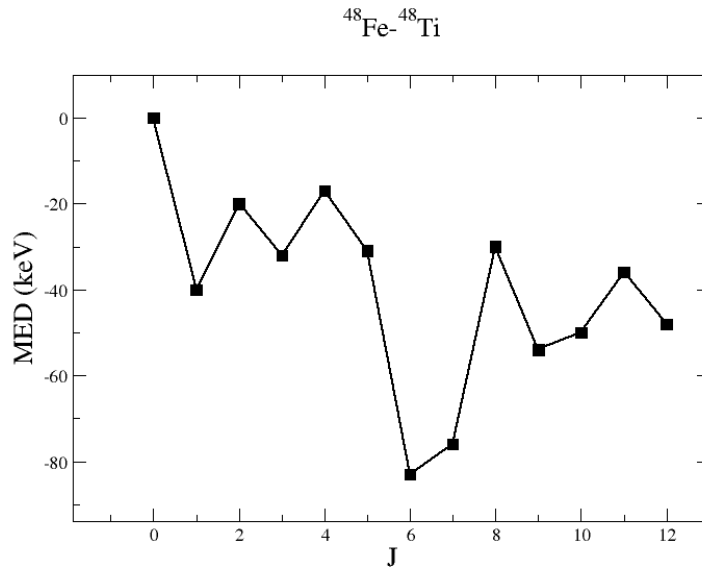


**Figure 5.14** Calculated MEDs of  $^{48}\text{Fe}$  and  $^{48}\text{Ti}$  with Coulomb interactions.

This also gives a prediction on the MEDs between  $^{48}\text{Fe}$  and  $^{48}\text{Ti}$  with the *gx1acdpn* interaction in the *fppn* model space using the NuShellX@MSU, which can be used in the further study in the MEDs between  $^{48}\text{Fe}$  and  $^{48}\text{Ti}$ .

## Chapter IV

# Summary and outlook

In this project, calculations of the yrast energy levels of several nuclei based on the  ${}^{40}_{20}\text{Ca}_{20}$  core are carried out using NuShellX@MSU code. The nuclei include  ${}^{42}_{20}\text{Ca}_{22}$ ,  ${}^{42}_{22}\text{Ti}_{20}$ ,  ${}^{42}_{21}\text{Sc}_{21}$ ,  ${}^{48}_{24}\text{Cr}_{24}$  and  ${}^{48}_{26}\text{Fe}_{22}$ . Furthermore, the MEDs between  ${}^{42}_{22}\text{Ti}_{20}$ - ${}^{42}_{20}\text{Ca}_{22}$ ,  ${}^{48}_{25}\text{Mn}_{23}$ - ${}^{48}_{23}\text{V}_{25}$ ,  ${}^{48}_{26}\text{Fe}_{22}$ - ${}^{48}_{22}\text{Ti}_{26}$  are also calculated.

When calculating  ${}^{42}_{20}\text{Ca}_{22}$ ,  ${}^{42}_{22}\text{Ti}_{20}$ ,  ${}^{42}_{21}\text{Sc}_{21}$ , several interactions in the model space  $f7pn$  and  $fp$  are used, selecting  $f742pn$  and  $fpmcc$  as the interaction types fitting the experimental results best respectively. Through the calculation of  ${}^{22}\text{Ca}$  and  ${}^{22}\text{Ti}$ , the interaction types  $f742pn$  and  $fpmcc$  are proved to be constructed without any Coulomb interactions. The existence of the Pauli exclusion principle is verified by the calculation results of  ${}^{42}\text{Sc}$  as the 7+ energy level occur in the spectra.

The interaction type  $fpmce$  in the  $fp$  model space is introduced to obtain better calculation results of  ${}^{48}\text{Cr}$ , which is a modification to the  $fpmcc$ . The rotational behavior and backbending of the  ${}^{48}\text{Cr}$  nucleus are also found in the spectra.

With the introduction of the  $gx1acdpn$  interaction in the  $fppn$  model space, the Coulomb effect is involved in the calculations of  ${}^{48}\text{Cr}$ . The prediction on the energy levels of  ${}^{48}\text{Fe}$  with and without the Coulomb interaction is then calculated with  $fpmce$  and  $gx1acdpn$ .

Finally, the MEDs calculated between  ${}^{42}_{22}\text{Ti}_{20}$ - ${}^{42}_{20}\text{Ca}_{22}$ ,  ${}^{48}_{25}\text{Mn}_{23}$ - ${}^{48}_{23}\text{V}_{25}$  show the isospin symmetry breaking brought by the Coulomb interactions. However, due to the lack of other components in the isospin symmetry breaking, the calculated MEDs does not fit the experimental MEDs very well, but they show the same tendency. And the MEDs between  ${}^{48}\text{Fe}$  and  ${}^{48}\text{Ti}$  are predicted using the  $gx1acdpn$  interaction.

With all the calculation results, one can understand the nuclear physics and the nuclear shell model mechanism better. The predictions can be useful to the Lund nuclear structure group for future experiments as well. To study the self-bound interacting fermions with further steps, one can try more interactions from different model spaces to see how the modifications in the interaction types can affect the output results or even make some improvements.

# References

- [1] M. Brack, J. Damgaard, A. S. Jensen *et al.*, *Rev. Mod. Phys.* 44, 320 (1972).
- [2] O. Sorlin and M.-G. Porquet, *Prog. Part. Nucl. Phys.* 61, 602 (2008).
- [3] B. A. Brown and B. H. Wilden, *Ann. Rev. Nucl. Part. Sci* 38, 29 (1988).
- [4] William Rae, NuShellX. <http://www.garsington.eclipse.co.uk/>.
- [5] B. A. Brown and W. D. M. Rae, *Nucl. Data Sheets* 120, 115 (2014).
- [6] The OEIS Foundation Inc., Rutherford's Nuclear World: The Story of the Discovery of the Nucleus.  
<https://history.aip.org/history/exhibits/rutherford/sections/alpha-particles-atom.html>.
- [7] Introduction to Nuclear Physics.  
<https://www.vanderbilt.edu/AnS/physics/brau/H182/Introduction%20to%20Nuclear%20Physics.pdf>.
- [8] R. H. Petrucci, Nuclear Magic Numbers - Chemistry LibreTexts.  
[https://chem.libretexts.org/Core/Physical\\_and\\_Theoretical\\_Chemistry/Nuclear\\_Chemistry/Nuclear\\_Energetics\\_and\\_Stability/Nuclear\\_Magic\\_Numbers](https://chem.libretexts.org/Core/Physical_and_Theoretical_Chemistry/Nuclear_Chemistry/Nuclear_Energetics_and_Stability/Nuclear_Magic_Numbers).
- [9] M. G. Mayer, *Phys. Rev.* 75, 1969 (1949).
- [10] O. Haxel, J. H. D. Jensen, and H. E. Suess, *Phys. Rev.* 75, 1766 (1949).
- [11] W. E. Meyerhof, *Lect. Elem. Nucl. Phys. Phys. Nucl. Part.* 1018, (2004).
- [12] The OEIS Foundation Inc., A018226. <https://oeis.org/A018226>.
- [13] J. A. Nolen Jr and J. P. Schiffer, *Annu. Rev. Nucl. Sci.* 19, 471 (1969).
- [14] Jonas C. Cremon, *Quantum Few-Body Physics with the Configuration Interaction Approach - Method Development and Application to Physical Systems*, Lund University, 2010.
- [15] National Nuclear Data Center, ADOPTED LEVELS, GAMMAS for  $^{42}\text{Ca}$ .  
<https://www.nndc.bnl.gov/chart/getdataset.jsp?nucleus=42CA&unc=nds>.
- [16] National Nuclear Data Center, ADOPTED LEVELS, GAMMAS for  $^{48}\text{Cr}$ .  
<https://www.nndc.bnl.gov/chart/getdataset.jsp?nucleus=48CR&unc=nds>.
- [17] S. J. Q. Robinson, A. Escuderos, L. Zamick *et al.*, *Phys. Rev. C* 73, 37306 (2006).
- [18] S. Raman, C. W. Nestor, and P. Tikkanen, *At. Data Nucl. Data Tables* 78, 1 (2001).
- [19] A. Juodagalvis and S. Åberg, *Phys. Lett. B* 428, 227 (1998).
- [20] J. B. McGrory and B. H. Wildenthal, *Phys. Lett. B* 103, 173 (1981).

- [21] National Nuclear Data Center, ADOPTED LEVELS, GAMMAS for  $^{48}\text{Fe}$ .  
<https://www.nndc.bnl.gov/chart/getdataset.jsp?nucleus=48FE&unc=nds>.
- [22] M. Honma, T. Otsuka, B. A. Brown, and T. Mizusaki, *Eur. Phys. J. A* 25, 499 (2005).
- [23] A. P. Zuker, S. M. Lenzi, G. Martínez-Pinedo, and A. Poves, *Phys. Rev. Lett.* 89, 142502 (2002).
- [24] J. Ekman, *Mirror Nuclei-Isospin Symmetry Breaking in the Mass A=35 and A=51 Mirror Nuclei*, Lund University, 2004.
- [25] National Nuclear Data Center, ADOPTED LEVELS, GAMMAS for  $^{48}\text{Mn}$ .  
<https://www.nndc.bnl.gov/chart/getdataset.jsp?nucleus=48MN&unc=nds>.